Astron. Astrophys. 327, 736–742 (1997)

ASTRONOMY AND ASTROPHYSICS

On the mass distribution of planetary nebulae central stars⋆

G. Stasińska[1], **S.K. Górny**[2], **and R. Tylenda**[2,3]

[1] DAEC, Observatoire de Meudon, F-92195 Meudon Principal Cedex, France (e-mail: grazyna@obspm.fr)
[2] Copernicus Astronomical Center, Laboratory of Astrophysics, ul. Rabiańska 8, PL-87-100 Toruń, Poland
(e-mail: skg@ncac.torun.pl, e-mail: tylenda@ncac.torun.pl)
[3] Toruń Center for Astronomy, Nicolaus Copernicus University, PL-87-100 Toruń, Poland

Received 21 February 1997 / Accepted 26 May 1997

Abstract. We apply a method, described in Górny et al. (1997), to derive the masses of 125 central stars of planetary nebulae (PN). This method is self-consistent and distance-independent. It requires the knowledge of the nebular Hβ fluxes, angular radii and expansion velocities, as well as the stellar visual magnitudes. This method is based on a simple model for the evolution of planetary nebulae, in which the central stars evolve according to the theoretical models of Blöcker (1995) and Schönberner (1983). The results are dependent on the assumed *total* nebular mass. Nevertheless, for any reasonable *total* nebular mass distribution, we find that the range in planetary nebulae central star masses is very restricted: more than 80% of the objects have a central star mass between 0.55 and 0.65M$_\odot$. We show how to convert, in this mass range, the observed PN central star mass distribution into a zero-age post-AGB star mass distribution.

Key words: planetary nebulae: general – stars: AGB and post-AGB – stars: white dwarfs – stars: fundamental parameters

1. Introduction

The central stars of planetary nebulae (hereinafter PN) are believed to be the immediate precursors of white dwarfs, and the remnants cores of intermediate-mass stars which have lost most of their mass through stellar winds while on the AGB. Together with the white dwarf mass distribution (Weidemann 1990), the shape of the mass distribution of planetary nebulae nuclei (hereinafter PNN) provides constraints on the theory of stellar evolution, as well as on models of galactic evolution that are based on it.

Histograms of the distribution of PNN masses have been published by several authors (Schönberner 1981, Heap & Augensen 1987, Weidemann 1989, Tylenda et al. 1991, Zhang & Kwok 1993). They all agree that the distribution of central star masses is rather narrow, roughly concentrated around 0.60M$_\odot$, and exhibits a strong cutoff at 0.55M$_\odot$. However, the exact value of the average PNN mass varies from one paper to another, and the proportion of PN with nuclei more massive than 0.7M$_\odot$ ranges from a few percent (Schönberner 1981) to 40% (Kaler et al. 1990). The problem of the studies mentioned above is that they make assumptions on the nebulae, which are not always explicit, thus making more difficult the discussion of the results.

In a previous work (Górny et al. 1997, hereinafter GST97), we have proposed a method to estimate PNN masses in which the assumptions were clearly stated. We applied it to a sample of PN for which we could assign a morphological class, in order to investigate any possible relation between the morphology and the central star masses. We now use the method for a larger sample of Galactic PN. The procedure and the observational data base are described in Sect. 2. The resulting distribution of PNN masses is presented and discussed in Sect. 3. Concluding remarks are given in Sect. 4.

2. Derivation of the PNN masses

2.1. Summary of the method

The method is extensively described in GST97, and we give here only the essentials. The basic idea - shared by all the methods for deriving PNN masses - is that central stars of different masses M_* differ in their basic properties (effective temperature T_* and total luminosity L_*) at any time t. The PNN masses can then be estimated by comparing the observed nuclei with a grid of evolutionary models of post-AGB stars of different M_*. Since, generally, the available observations do not allow a direct determination of T_* and L_* and of the time, t, one uses the surrounding nebulae to approach the physical properties of the central star. However, the parameters one recovers are generally different from T_*, L_* and t, mainly because the distance to the PN is unknown and because the nebula may be ionization- or density-bounded.

Our approach is to compare the properties of the observed objects with those of simple models which receive exactly the same treatment as the observations in the estimation of L_*, T_*

Send offprint requests to: S.K. Górny

⋆ Table 1 is available in electronic form at the CDS via anonymous ftp 130.79.128.5

and t. Our models consist of a spherical nebula of given total mass M_{neb} expanding at a constant velocity v_{exp} around an evolving star of mass M_*. The covering factor is taken equal to 1, the thickness of the gaseous shell is $\Delta R/R$ = 0.3 and the density is uniform. The central star evolution is interpolated from the theoretical grid of Blöcker (1995) and Schönberner (1983), relevant for H-burning central stars, which are believed to constitute the majority of PNN. A blackbody radiation field is assumed. We can then compute at each time, the radius and mass of the ionized part of the nebula, and its luminosity in Hβ.

In the traditional H-R diagram, if the stellar temperature and luminosity are obtained by the Zanstra method using the Shklovsky distance, this amounts to comparing the positions of the objects to "apparent" theoretical tracks for stars of different masses. These apparent tracks differ significantly from the pure stellar tracks (see Fig. 1a below), and are strongly dependent on v_{exp} and M_{neb} (see GST97). This is why the conclusions on PNN masses derived by authors using the H-R diagram (e.g. Kaler et al. 1990, Stanghellini et al. 1993, Cazetta & Maciel 1994) need to be reexamined. A similar comment applies to the $(M_{\rm v}, t)$ diagram (used by Schönberner 1981, Heap & Augensen 1987 and Weidemann 1989) where $M_{\rm v}$ is the stellar absolute visual magnitude.

Many PN have their expansion velocity measured. Such objects can be directly compared with a grid of apparent tracks built with the same v_{exp} as observed. The only unknown parameter in our approach is M_{neb}, and the estimated value of M_* depends on the assumed M_{neb}. The advantage of our method is that it is self-consistent and that all the assumptions can be clearly stated.

2.2. The sample of PN

We have considered all the PN for which the relevant data (stellar apparent visual magnitude $m_{\rm v}$, total nebular flux F(Hβ), nebular angular radius θ and expansion velocity v_{exp}) are available in the literature and of good quality, and for which the central stars are not known to be close binaries or to have H-poor atmospheres. The observational data, together with the references, are listed in Tylenda & Stasińska (1994), and we use the same extinction correction procedure as in that paper. This results in a sample of 125 objects.

Fig. 1a shows all these objects in the $(L(Z_{\rm H}, Sh), T(Z_{\rm H}))$ plane, where $T(Z_{\rm H})$ is the Zanstra temperature of the star derived from the Hβ line, and $L(Z_{\rm H}, Sh)$ is its Zanstra luminosity calculated with the Shklovsky distance. Superimposed are the apparent tracks for central stars of masses 0.565, 0.605 and 0.645M$_\odot$, surrounded by a nebula of *total* mass 0.2M$_\odot$ whose outer rim is expanding at 20km/sec (continuous curves). The Zanstra luminosity and temperature of the central star, as well as the Shklovsky distance are derived in exactly the same way as in the observations (i.e. assuming a *shining* mass of 0.2M$_\odot$ and a filling factor of 0.5). For illustration, we also show (dotted curves) the original theoretical tracks for the same stars, that is the variations of L_* as a function of T_*.

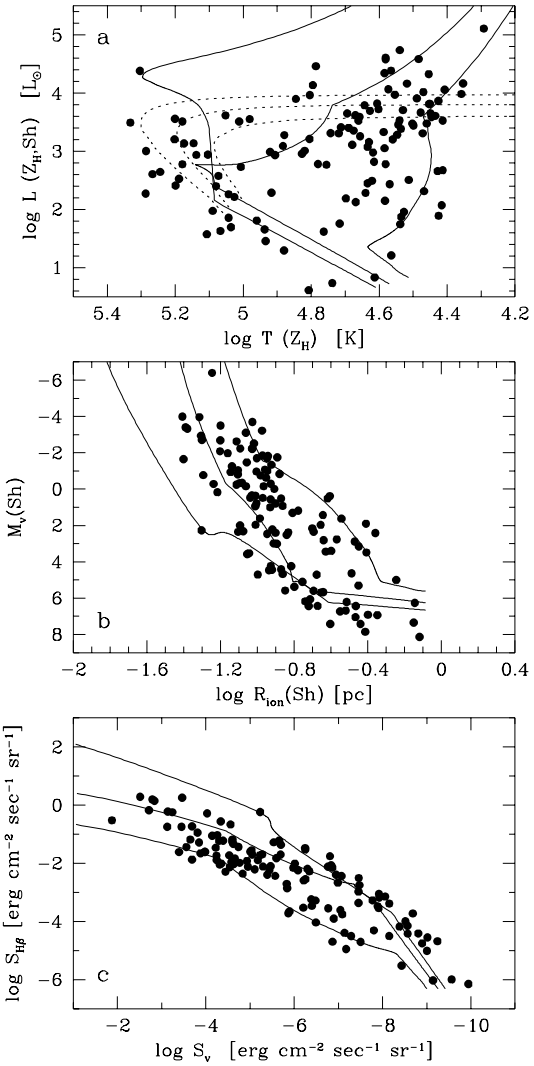

Fig. 1a–c. Distribution of PN in three analyzed diagrams. **a** Zanstra luminosity, $L(Z_{\rm H}, Sh)$, (in solar units) calculated with the Shklovsky distance, versus Zanstra temperature, $T(Z_{\rm H})$, (in Kelvins). Observed PN are represented by circles. Continuous curves: apparent tracks (see text) for central stars of masses 0.565, 0.605 and 0.645M$_\odot$, surrounded by a nebula of 0.2M$_\odot$ expanding at 20km/sec. Dotted curves: the original theoretical tracks for the same stars, i.e. the variations of L_* as a function of T_*. **b** Total visual magnitude of the central stars, $M_{\rm v}(Sh)$, calculated at the Shklovsky distance, versus radius of the ionized part of the nebula, $R_{ion}(Sh)$ (in pc). **c** Nebular surface brightness in Hβ, $S_{\rm H\beta}$, versus $S_{\rm v}$ (see text).

Fig. 1b is similar to Fig. 1a but in the $(M_{\rm v}(Sh), R_{ion}(Sh))$ plane, where $M_{\rm v}(Sh)$ is the absolute stellar visual magnitude, and $R_{ion}(Sh)$ the radius of the ionized part of the nebula, both calculated with the Shklovsky distance. Fig. 1c shows the same, but in the $(S_{\rm H\beta}, S_{\rm v})$ plane introduced by GST97, where $S_{\rm H\beta}$ is the nebular surface brightness in Hβ, and $S_{\rm v}$ is defined as $F_{\rm v}/(\pi\theta^2)$, where $F_{\rm v}$ is the stellar flux in the V band.

Note that not only Fig. 1c is distance independant. Figs. 1a and 1b are also independent of the true distances, since they

Table 1. Planetary nebulae properties and derived central stars masses, evolutionary ages and distances

PN G	Main Name	type	log $T(Z_{\rm H})$	log $L(Z_{\rm H}, Sh)$	$M_{\rm v}(Sh)$	log $R_{ion}(Sh)$	log $S_{\rm v}$	log $S_{{\rm H}\beta}$	$d_{\rm Sh}$	M_*	t_{ev}	d
002.0−13.4	IC 4776		4.67	3.36	0.36	-1.01	-5.05	-1.70	5.4	0.581	6.7	5.4
018.0+ 20.1	Na 1	E:	4.63	3.08	0.79	-0.90	-5.44	-2.23	6.5	0.605	4.3	6.5
027.6−09.6	IC 4846		4.64	3.79	-0.94	-1.15	-4.26	-1.02	10.2	0.579	5.2	9.1
034.6+ 11.8	NGC 6572		4.84	3.90	0.17	-1.22	-4.56	-0.66	2.5	0.607	3.6	2.2
035.9−01.1	Sh 2- 71	I	4.47	2.31	1.62	-0.54	-6.49	-4.03	1.1	0.564	15.6	1.1
045.4−02.7	Vy 2- 2		4.54	4.74	-4.00	-1.41	-2.51	0.29	26.9	0.613	1.6	9.6
047.0+ 42.4	A 39	EH	4.56	1.21	5.00	-0.25	-8.43	-5.52	1.4	0.575	16.8	1.4
051.4+ 09.6	Hu 2-1		4.58	4.34	-2.71	-1.30	-3.24	-0.24	11.4	0.589	3.6	5.7
052.5−02.9	Me 1-1	B	4.53	3.71	-1.47	-1.06	-4.22	-1.46	7.7	0.562	9.1	6.5
057.2−08.9	NGC 6879	E	4.54	3.46	-0.76	-0.98	-4.66	-1.83	8.6	0.585	4.5	8.6
058.3−10.9	IC 4997		4.79	4.46	-1.65	-1.40	-3.47	0.26	10.2	0.617	2.0	5.1
060.1−07.7	NGC 6886	BE:	5.05	3.62	2.35	-1.10	-5.66	-1.22	5.9	0.619	3.3	5.9
074.5+ 02.1	NGC 6881	B	4.80	3.97	-0.29	-1.24	-4.34	-0.56	9.2	0.607	3.4	7.5
082.5+ 11.3	NGC 6833		4.58	4.58	-3.32	-1.38	-2.84	0.15	34.4	0.601	2.6	13.9
084.9+ 04.4	A 71	E	5.04	1.70	7.04	-0.47	-8.81	-4.41	0.9	0.883	20.8	0.9
086.5−08.8	Hu 1-2	B	4.98	3.55	2.00	-1.09	-5.54	-1.28	5.1	0.621	2.8	5.1
093.3−02.4	M 1-79	B:	5.04	2.26	5.68	-0.65	-7.89	-3.48	2.9	0.607	9.3	2.9
096.4+ 29.9	NGC 6543		4.66	3.59	-0.34	-1.08	-4.62	-1.33	1.7	0.595	4.2	1.7
100.0−08.7	Me 2-2	E	4.79	4.14	-0.77	-1.29	-4.03	-0.28	17.5	0.603	3.8	11.5
100.6−05.4	IC 5217		4.72	3.31	0.78	-1.00	-5.23	-1.72	6.3	0.607	4.0	6.3
102.8−05.0	A 80	BE:	5.11	1.57	7.85	-0.41	-9.24	-4.68	1.2	>0.940	-	-
104.8−06.7	M 2-54	E	4.29	5.11	-6.40	-1.25	-1.88	-0.52	23.4	0.563	4.1	4.1
107.6−13.3	Vy 2- 3	E	4.46	3.48	-1.34	-0.92	-4.54	-2.13	10.9	0.562	8.2	10.9
111.8−02.8	Hb 12	E	4.58	4.61	-3.40	-1.39	-2.79	0.20	24.0	0.609	2.1	9.7
112.9−10.2	A 84	BE:	4.93	1.46	6.92	-0.40	-8.89	-4.75	1.4	0.866	19.5	1.4
118.0−08.6	Vy 1- 1	E	4.50	3.44	-1.01	-0.95	-4.63	-2.02	7.8	0.562	10.9	7.8
119.6−06.7	Hu 1-1	E:	5.10	2.94	4.41	-0.87	-6.95	-2.39	5.6	0.609 (0.654)	6.5	5.6
130.3−11.7	M 1- 1	E:	4.58	3.05	0.52	-0.87	-5.39	-2.39	11.1	0.607	3.6	11.1
130.4+ 03.1	K 3-92	B	4.67	2.13	3.40	-0.60	-7.09	-3.75	8.5	0.561	41.1	8.5
158.8+ 37.1	A 28		4.74	0.73	7.34	-0.15	-9.56	-5.99	1.0	>0.940	-	-
158.9+ 17.8	PuWe 1		4.81	0.61	8.13	-0.12	-9.94	-6.15	0.3	>0.940	-	-
159.0−15.1	IC 351	E:	4.68	3.11	1.00	-0.93	-5.47	-2.10	6.9	0.593	6.0	6.9
167.4−09.1	K 3-66		4.47	4.02	-2.63	-1.11	-3.65	-1.18	15.1	0.583	3.0	10.8
171.3−25.8	Ba 1	E	4.72	1.76	4.63	-0.49	-7.80	-4.31	3.4	0.599	8.8	3.4
189.8+ 07.7	M 1- 7	B	5.01	2.73	4.24	-0.82	-6.99	-2.67	6.3	0.589	10.6	6.3
210.3+ 01.9	M 1- 8	B	5.19	2.53	6.07	-0.71	-7.93	-3.18	4.3	0.776	16.1	3.2
212.0+ 04.3	M 1- 9	E	4.61	3.82	-1.26	-1.14	-4.15	-1.05	13.0	0.569	6.1	10.6
220.3−53.9	NGC 1360		4.54	1.87	3.15	-0.45	-7.29	-4.50	0.4	0.577	12.4	0.4
226.7+ 05.6	M 1-16		4.66	3.53	-0.16	-1.06	-4.74	-1.44	9.9	0.567	8.3	9.9
248.7+ 29.5	A 34		4.61	0.83	6.26	-0.14	-9.14	-6.03	1.0	0.626	20.6	1.0
283.6+ 25.3	K 1-22		4.88	1.29	6.93	-0.35	-9.01	-5.01	1.0	0.877	15.7	1.0
288.8−05.2	He 2- 51		4.47	3.31	-0.84	-0.88	-4.83	-2.35	6.1	0.561	12.7	6.1
318.4+ 41.4	A 36		4.42	1.89	2.42	-0.36	-7.17	-4.95	0.5	0.575	11.9	0.5
320.1−09.6	He 2-138		4.41	4.06	-3.11	-1.06	-3.56	-1.44	5.1	0.562	6.9	2.9
321.8+ 01.9	He 2-120		5.24	2.65	6.18	-0.74	-7.92	-3.05	2.8	0.881	23.5	1.9
325.8−12.8	He 2-182		4.55	3.97	-1.98	-1.16	-3.81	-0.94	9.5	0.595	2.9	7.5
326.0−06.5	He 2-151		4.35	4.17	-3.70	-1.03	-3.39	-1.61	12.9	0.557	19.7	5.8
329.0+ 01.9	Sp 1		4.51	2.51	1.42	-0.64	-6.21	-3.53	1.3	0.587	7.4	1.3
331.4−03.5	He 2-162		4.36	3.99	-3.22	-0.97	-3.69	-1.87	8.7	0.560	10.3	5.2

use the "Shklovsky distance", which is a mere combination of observed parameters.

2.3. The PNN masses of our sample

As stated above, the only parameter on which we do not have any observational constraint in our representation is the total nebular mass. We derive the central star masses, M_*, assuming a total nebular mass of $0.2{\rm M}_\odot$. Table 1 (available also in electronic form) gives the values of M_* for all the PN of our sample that do not appear in Table 1 of GST97. If more than one value of M_* is possible for a given object, the lowest value is adopted, and the upper limit compatible with the data is indicated in parenthesis. As an information, Table 1 also lists, in the same format as Table 1 of GST97, the values of the following parameters: the morphological type as defined in GST97[1], log $T(Z_{\rm H})$, log $L(Z_{\rm H}, Sh)$ (in solar units), $M_{\rm v}(Sh)$, log $R_{ion}(Sh)$ (in pc), log $S_{\rm v}$ (in erg cm^{-2} sec^{-1} sr^{-1}), log $S_{{\rm H}\beta}$ (in erg cm^{-2} sec^{-1} sr^{-1}), the Shklovsky distance d_{Sh} (in kpc), as well as the evolutionary time t_{ev}(in units of 10^3yrs) and the distance d (in kpc) (the latter two parameters being obtained once M_* has been determined, as explained in GST97).

The uncertainty in PNN mass resulting from a change in M_{neb} by a factor two downwards or upwards is represented in Fig. 2a. We see that, for most objects, it becomes important only if M_* is larger than about $0.65{\rm M}_\odot$. At high central masses, the uncertainty may become very large if the PN is in an evolutionary stage corresponding to a region of crowding of apparent tracks.

The effects of the observational uncertainties in F(Hβ), θ and $m_{\rm v}$ on the determination of M_* are of $\pm 0.01{\rm M}_\odot$ at most for $M_*<0.65{\rm M}_\odot$. They are much larger at higher central star masses. One may consider that for $M_*>0.65{\rm M}_\odot$, the problem of deriving central star masses with our method becomes degenerate, and that masses above $0.65{\rm M}_\odot$ are very uncertain.

[1] In addition to the sources quoted in GST97 for the PN images, we also analyzed the recent catalogue of Manchado et al.(1996)

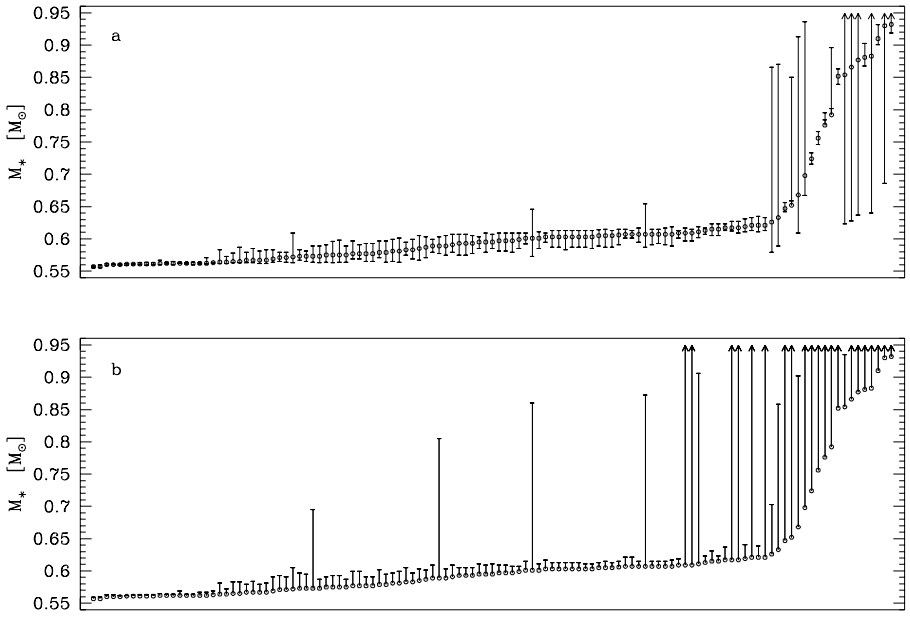

Fig. 2. a The uncertainty in PNN mass resulting from a change of M_{neb} by a factor two downwards or upwards. Taking a higher M_{neb} results in a lower derived PNN mass (in all but two cases). The objects are ordered by increasing M_* (value obtained assuming M_{neb}=0.2M$_\odot$). **b** The uncertainty in PNN mass resulting from using a different covering factor. Circles: PNN masses obtained with M_{neb}=0.2 and a covering factor of 1. Dashes (or arrows): PNN masses (or limits) obtained with M_{neb}=0.2 and a covering factor of 0.3.

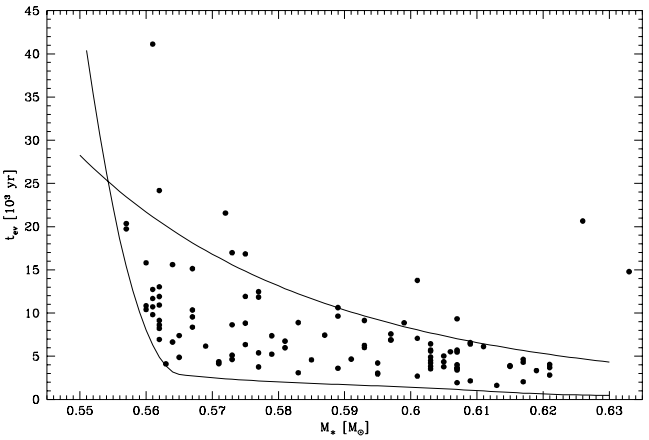

Fig. 3. Estimated age t_{ev}, as a function of PNN mass M_* (assuming M_{neb}=0.2M$_\odot$) for objects with M_*<0.64M$_\odot$.

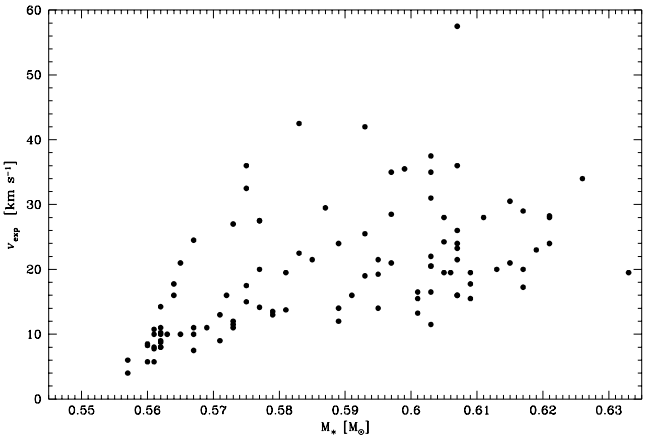

Fig. 4. Observed PN expansion velocity, v_{exp} as a function of PNN mass M_* (assuming M_{neb}=0.2M$_\odot$) for objects with M_*<0.64M$_\odot$.

Additional causes of uncertainty are of course deviations from our adopted model. For instance, masses derived under the assumption of a covering factor smaller than one are larger than if the covering factor is assumed equal to one. Fig. 2b shows the effect of adopting a covering factor of 0.3 for all the PN. While this leaves practically unchanged the derived central star masses at $M_* < 0.56$M$_\odot$ and some of those at about 0.60M$_\odot$, it may increase significantly the derived masses in other cases, especially those with $M_* > 0.65$M$_\odot$. Actually, the true covering factor of many PN is probably close to one, so that the errors are not as large as Fig. 2b might express. Covering factors drastically smaller than one are expected for some bipolar PN (those of subclass *B* following the nomenclature of GST97), whose proportion among PN with $M_* < 0.65$M$_\odot$ is rather small (see GST97), and for irregular PN, which constitute only a small fraction of the PN.

In Fig. 3, we plot the values of the evolutionary time t_{ev}, as a function of M_* (assuming M_{neb}=0.2M$_\odot$), for the low M_* objects of our sample. We see a trend similar to the one found in GST97. PN with small M_* (around 0.56M$_\odot$) are seen at ages between from 5000 years to over 20000 years. PN with M_* about 0.62M$_\odot$ are seen between 2000 and 5000 years. Two curves are drawn in Fig. 3. The lower one represents the time when central stars have a temperature of 20000K. The other one, which is a sort of upper envelope of the PN ages in our sample, was obtained by dividing the sample into 5 bins of approximately 20 objects each, and by drawing a smooth curve below which are found 90% of the objects in each bin. One can see that both curves decrease with M_*. The behaviour of the lower one simply reflects that low mass PNN evolve more slowly and become able to ionize the surrounding nebula only at larger ages. The behaviour of the upper curve is better understood when considering Fig. 4, which represents v_{exp} as a function

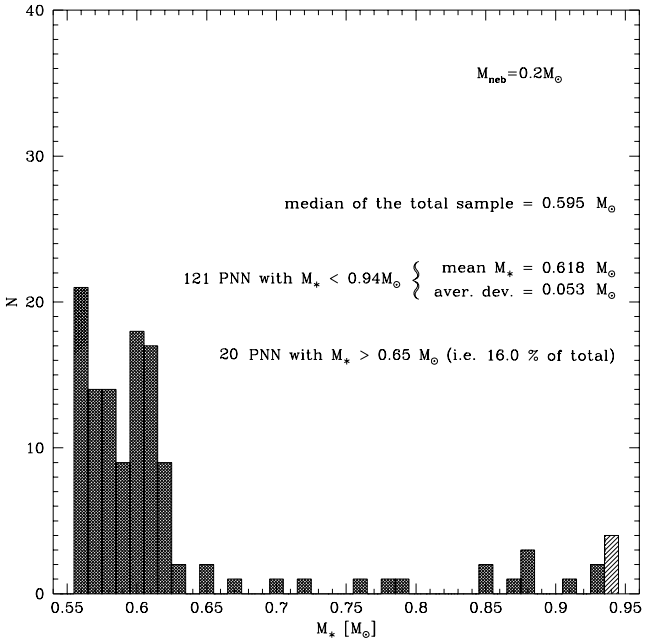

Fig. 5. Histogram of the PNN mass distribution (adopting M_{neb}=0.2 $M_\odot$) for our sample of PN. The light shadowed bar includes objects for which only the lower mass limit (M_*>0.94$M_\odot$) could be derived.

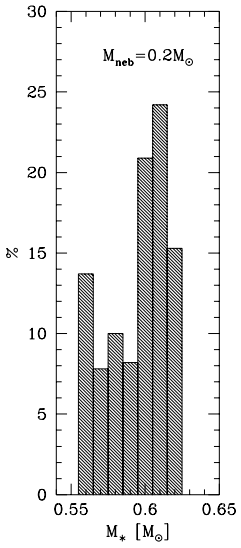

Fig. 6. Histogram of the zero-age post-AGB stars derived from Fig. 5 (see text).

of M_*. This plot confirms the trend shown in GST97 that, for objects with $M_* < 0.62M_\odot$, v_{exp} tends to be larger for PN with nuclei of larger masses. Thus, at the same age, PN with central stars of higher masses tend to be more diluted, which discriminates against them in a sample where the Hβ fluxes have to be measured.

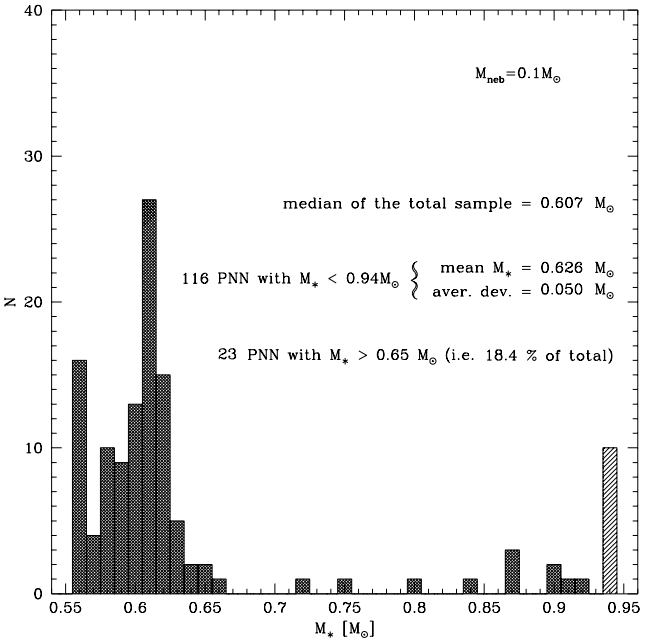

Fig. 7. Histogram of the PNN mass distribution (adopting M_{neb}=0.1 $M_\odot$) for our sample of PN.

3. The distribution of PNN masses

Fig. 5 shows the histogram of the PNN mass distribution we find for our sample using M_{neb}=0.2 $M_\odot$. The median, mean and the average deviation of the distribution of PNN masses below 0.94$M_\odot$ are indicated in the figure, together with the number of objects. The proportion of objects with derived PNN masses above 0.65$M_\odot$ is also indicated. We see that the obtained distribution is very narrow, with more than 80% of the objects having M_* between 0.55 and 0.65$M_\odot$. There are no objects with M_* below 0.555$M_\odot$. This is simply due to the selection effect that stars with smaller masses evolve so slowly that the nebular envelope would disperse before the star gets hot enough to ionize it. On the other hand, as in many of the studies devoted to this problem, we find a long (but not very numerous) tail with PNN masses above 0.65$M_\odot$.

Because the lifetime of the PN phenomenon is depending on M_*, the *observed* distribution of PN central star masses does not reflect the distribution of masses of post-AGB stars. Using our Fig. 3, we can empirically determine the mass distribution of zero-age post-AGB stars between 0.555$M_\odot$ and 0.625$M_\odot$. It is simply obtained by dividing in each mass bin the number of objects by the characteristic time interval between the upper and lower envelope of the bulk of PN ages represented by the two curves in Fig. 3. The resulting distribution is shown in Fig. 6.

It is obviously quite different from the one displayed in Fig. 5, by having a much larger proportion of objects with higher M_*. Because the number of objects in each mass bin above 0.625 $M_\odot$ is so small, and because the M_* determinations are so uncertain at such high masses, the distribution of post-AGB star masses above 0.625$M_\odot$ cannot be derived quantitatively. Hovewer, the small number of observed PN with M_*>0.65$M_\odot$

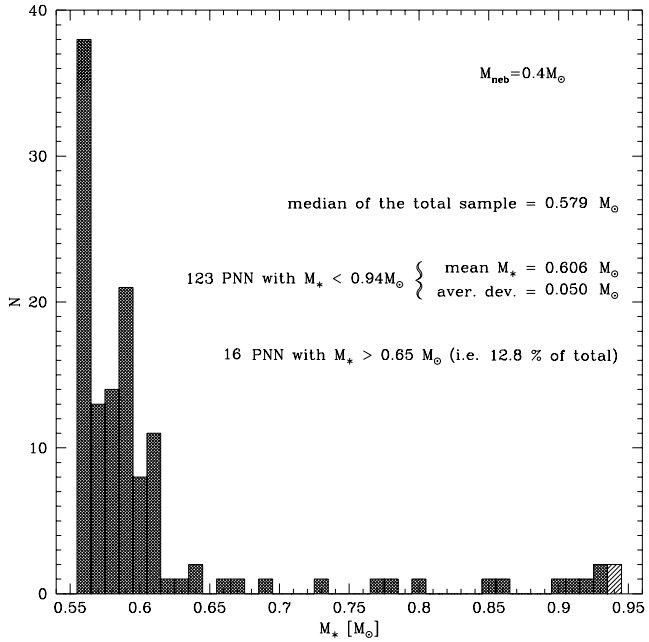

Fig. 8. Histogram of the PNN mass distribution (adopting M_{neb}=0.4 $M_\odot$) for our sample of PN.

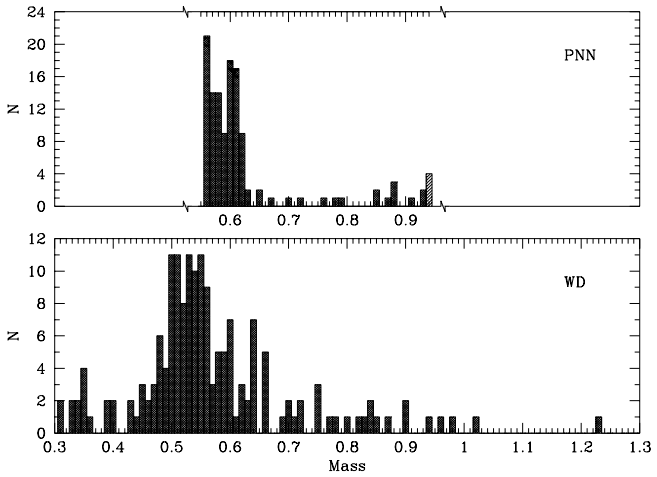

Fig. 9. Bottom: histogram of the white dwarf mass distribution from the works of Bergeron et al. (1992) and Bragaglia et al. (1995). Top: Histogram of the PNN mass distribution of Fig. 5 represented on the same horizontal scale.

indicates that there must be a drop in the post-AGB star mass distribution at about this mass.

One must not forget, however, that our M_* determinations were made under the assumption that M_{neb}=0.2$M_\odot$. A different choice for M_{neb} would lead to a different determination of the PNN masses. Fig. 7 shows the histogram of PNN masses we derive under the assumption that M_{neb}=0.1 $M_\odot$, and Fig. 8 shows the histogram obtained under the assumption that M_{neb}=0.4 $M_\odot$. The characteristics of the distributions (median, mean, etc... are indicated in the same way as in Fig. 5). As mentioned above and in GST97, the derived PNN masses are higher for a smaller assumed M_{neb}. Note that also the shape of the PNN mass distributions varies when changing the assumption on M_{neb}. For an assumed M_{neb} of 0.4$M_\odot$, about 30% of the objects lie in the 0.555$\pm$0.005$M_\odot$ bin.

Undoubtedly, there must be a certain dispersion in the values of M_{neb} of real planetary nebulae. It seems that in the Galactic bulge PN, values around 0.1 - 0.15 $M_\odot$ are more probable for the total nebular mass (Stasińska & Tylenda 1994), while in the Magellanic Clouds, PN that are optically thin rather indicate a value of about 0.3$M_\odot$ (Barlow 1987). The conclusion of all this is that the true distribution of PN central stars or of zero-age post-AGB stars is impossible to determine accurately in absence of additional observational parameters.

It remains that the distribution of PN central star masses is very narrow, the vast majority of the objects having M_* between 0.55$M_\odot$ and 0.65$M_\odot$.

Whether the PN central star mass distribution is compatible with that of white dwarfs is a question which requires a detailed modelling of galactic evolution (similar to the work of Koester & Weidemann 1980, or Yuan 1989), together with an explicit modelling of the biases affecting the observations of white dwarfs and planetary nebulae. Such an enterprise is out of the scope of the present study. For illustrative purposes, we simply compare in Fig. 9 the PNN mass distribution of Fig. 5 and the white dwarf mass distribution as obtained from the works of Bergeron et al. (1992) and Bragaglia et al. (1995). The fact that the white dwarf distributions extends to lower masses than the PNN mass distribution reflects in part the selection effects operating against the observation of planetary nebulae with very slowly evolving nuclei.

4. Concluding remarks

Using a self-consistent method based on a simple model of PN evolution, we have derived central star masses for a sample of 125 objects in which we could use the following observables: nebular Hβ flux, angular radius and expansion velocity, and stellar visual magnitude. Note that our approach does not require a knowledge of the distances to the objects. Our method can easily be generalized in the future to more realistic morphodynamical models for the evolution of PN.

We have shown how it is possible to empirically convert a distribution of central star masses of observed PN into a distribution of masses of zero-age post-AGB stars.

However, we also emphasized that the derived central star mass distribution depends on the - unknown - total nebular mass. Note that, even knowing the PN distances by independent means, such as expansion parallaxes (Hajian et al. 1995), would not suppress the uncertainty in the central star mass M_*, which is linked to the fact that we do not know by how much a given PN is density bounded. Actually, this uncertainty is present in all the previously published determinations of central star masses that rely on nebular properties, although not explicitely stated. It is only by using more realistic models for the PN evolution, together with additional observables that one could perhaps improve the situation.

Actually, the only way to obtain accurate central star masses would be by model fitting of high resolution spectra of these stars. This procedure, however, has its own uncertainties (see the different results obtained by Méndez et al. 1988 and 1992 for the same objects). Moreover, it is restricted to a small number of objects, as it is so demanding on the observational material as well as on the modelling procedure.

We find that in our sample more than 80% of the central stars have masses between 0.55 and 0.65$M_\odot$, the true distribution being probably narrower. The median value of M_* is ill defined, due to our absence of knowledge of the total nebular mass, which enters in the determination of M_* with our method. Of course, the values derived for the central star masses strongly depend on the assumed stellar evolution. Our determinations were made using the H-burning evolutionary tracks of Blöcker (1995) and Schönberner (1983).

Interpretation of the difference between the PNN mass distribution and that of related objects like white dwarfs requires a detailed galactic evolution modelling combined with a simulation of selection effects, and was not attempted here.

Acknowledgements. This research was partly supported by KBN (grant No. 2.P30D.027.10) and by CNRS: "jumelage France–Pologne".

References

Barlow M.J., 1987, MNRAS 227, 161
Bergeron P., Saffer R.A., Liebert J., 1992, ApJ 394, 228
Blöcker T., 1995, A&A 299, 755
Bragaglia A., Renzini A., Bergeron P., 1995, ApJ 443, 735
Cazetta J.O., Maciel W.J. 1994, A&A 290, 936
Górny S.K., Stasińska G., Tylenda R., 1997, A&A 318, 256 (GST97)
Hajian A.R., Terzian Y., Bignell C., 1995, AJ 109, 2600
Heap S.R., Augensen H.J., 1987, ApJ 313, 268
Kaler J.B., Shaw R.A., Kwitter K.B. 1990, ApJ 359, 392
Koester D., Weidemann V., 1980, A&A 81, 145
Manchado A.,Guerrero M.A., Stanghellini L., Serra-Ricart M., 1996, The IAC Morphological Catalogue of Northern Galactic Planetary Nebulae, IAC
Méndez R., Kudritzki R.P., Herrero A., 1992, A&A 260, 329
Méndez R., Kudritzki R.P., Herrero A., Husfeld D., Groth H.G., 1988, A&A 190, 113
Schönberner D., 1981, A&A 103, 119
Schönberner D., 1983, ApJ 272, 708
Stanghellini L., Corradi R.L.M., Schwarz H.E., 1993, A&A 279, 521
Stasińska G., Tylenda R., 1994, A&A 289, 225
Tylenda R., Stasińska G., 1994, A&A 284, 897
Tylenda R., Stasińska G., Acker A., Stenholm B., 1991, A&A 246, 221
Weidemann V. 1989, A&A 213, 155
Weidemann V., 1990, ARA&A 28, 103
Yuan J.W.,1989, A&A 224, 108
Zhang C.Y., Kwok S., 1993, ApJS 88, 137

This article was processed by the author using Springer-Verlag TEX A&A macro package version 3.